Carbon nanotubes effects on the relaxation properties and critical current densities of MgB_2 superconductor

G. Pasquini, A. Serquis, A. J. Moreno, G. Serrano, and L. Civale

Citation: Journal of Applied Physics **114**, 023907 (2013); doi: 10.1063/1.4813132
View online: https://doi.org/10.1063/1.4813132
View Table of Contents: http://aip.scitation.org/toc/jap/114/2
Published by the American Institute of Physics

JOURNAL OF APPLIED PHYSICS **114**, 023907 (2013)

Carbon nanotubes effects on the relaxation properties and critical current densities of MgB_2 superconductor

G. Pasquini,[1,a)] A. Serquis,[2] A. J. Moreno,[1] G. Serrano,[2] and L. Civale[3]
[1]*Departamento de Física, FCEN, Universidad de Buenos Aires, IFIBA, Conicet, Argentina*
[2]*Instituo Balseiro-Centro Atómico Bariloche, Conicet, S. C. de Bariloche 8400, Río Negro, Argentina*
[3]*Los Alamos National Laboratory, MS K764, Los Alamos, New Mexico 87545, USA*

(Received 16 April 2013; accepted 19 June 2013; published online 12 July 2013)

Addition of nonsuperconducting phases, such as carbon nanotubes, can modify the superconducting properties of MgB_2 samples, improving the critical current density and upper critical field. A full understanding of the flux creep mechanism involved is crucial to the development of superconducting magnets in persistent mode, one of the main thrusts for the development of MgB_2 wires. In this paper we present a creep study in bulk MgB_2 samples, pure and with different amounts of carbon nanotubes additions. We conclude that the most consistent picture at low temperatures is a single vortex pinning regime, where the correlation length is limited by the grain size. We introduce a novel analysis that allows us to identify the region where the Anderson-Kim model is valid. © *2013 AIP Publishing LLC*. [http://dx.doi.org/10.1063/1.4813132]

I. INTRODUCTION

Since the discovery of the superconductor MgB_2,[1] a lot of work was devoted to understand and to improve its pinning properties. The great potential for technological applications of this material is due to its high critical temperature T_c (~39 K), low cost of raw materials,[2] chemical simplicity, and absence of weak-link limitations to the critical current density J_c.[3] In the last years, several groups have achieved a good improvement of the transport properties. In bulk polycrystalline samples, good results for increasing J_c have been achieved by chemical doping or by the inclusion of nonsuperconducting phases, in particular with carbon nanotubes (CNT) inclusions,[4–9] with diameters close to the MgB_2 coherence length ξ. On the other hand, theoretical results predict and experimental studies confirm that the presence of two superconducting gaps produces significant H_{c2} enhancement in the dirty limit.[10] In a previous publication we have reported results in samples with double wall CNTs additions showing both effects: an important increase in the critical current density and the upper critical field H_{c2}.[7,8] However, it is not clear if this two effects are connected. Recent works have studied the activation energy in dirty MgB_2 samples, but the results are not conclusive.[11] In fact, the vortex physics underlying this performance improvement has not been so far understood.

In this paper we perform a deeper analysis of the role of naturally formed and artificially introduced pinning centers by studying the magnetic relaxation in bulk MgB_2 samples. The time decay rate of the supercurrents (flux creep rate), beyond its basic interest, is an important parameter for applications, particularly those involving the use of superconducting magnets in persistent mode, such as MRI, which is currently one of the main thrusts for the development of MgB_2 wires.[12]

As it is well known, if a superconducting sample in the critical state is fully penetrated by the magnetic field B, the magnetization M is proportional to the current density J flowing in the sample. The "measurable" critical current density J_c is lower than the "true" J_{c0} due to the thermal activated motion. In a magnetic relaxation experiment the measured J_c decays in time as

$$-\frac{\partial J_c}{\partial t} = C_j e^{\frac{-U(J_c,T,B)}{kT}}, \tag{1}$$

where $C_j \sim J_c/\tau_0$ can be approximated as a constant and $U(J_c,T,B)$ is the activation barrier.

In oxide High Temperature Superconductors (HTS), the creep drastically drops the measurable density current, so $J_c \ll J_{c0}$, an effect highly detrimental for applications. A large number of glassy creep regimes in this limit have been proposed theoretically,[13,14] and many of them observed experimentally.[15] In those cases the temperature dependence of the measurable critical current J_c is dominated by creep while the intrinsic $J_{c0}(T)$ dependence is much weaker. In recent years it has also became clear that iron-arsenide superconductors suffer from creep rates approximately as high as oxide HTS.[16] On the other hand, in traditional type II low temperature superconductors (LTS) superconductors the current decay is very small, so $J_{c0} - J_c \ll J_{c0}$; therefore, the activation barrier takes the traditional Anderson-Kim (A-K) linear dependence with the current density[17]

$$U(J_c,T,B) \simeq U_c(T,B)\left(1 - \frac{J_c}{J_{c0}(T,B)}\right), \tag{2}$$

where $U_c(T,B)$ is the pinning energy and $J_{c0}(T,B)$ would be the critical current density in the absence of creep.

From this basic point of view, MgB_2 is a very particular system, as the intermediate T_c and moderate anisotropy make the creep effects smaller than in HTS but larger than in conventional superconductors. From a technological

a)Electronic mail: pasquini@df.uba.ar

perspective, this puts MgB_2 in the rather unique situation of being the only known superconductor with high enough T_c to be easily operated in liquid-*He* free systems and at the same time sharing some important "LTS-like" advantages such as low creep rates, low anisotropy, and the absence of weak-links problems. The influence of thermal fluctuations in the vortex physics is measured by the Ginzburg number $Gi = (1/2)(kT_c/H_c^2\xi^3\varepsilon)^2$, where H_c is the thermodynamic critical field and $\varepsilon < 1$ is the effective mass anisotropy. For $YBa_2Cu_3O_{7-\delta}$ this is as large as $Gi \sim 10^{-2}$ and even larger for the more anisotropic *Bi*-based compounds, while for *NbTi*, the paradigmatic strong-pinning conventional superconductor, $Gi \sim 10^{-8}$. For MgB_2, depending on the doping level we have $Gi \sim 10^{-4} - 10^{-5}$. This is just in the middle between the extreme cases. The first consequence is that J_c is expected to be in the intermediate range $J_{c0} - J_c \lesssim J_{c0}$ and the A-K limit would be only valid at low temperature.

In this paper we present an experimental study in bulk MgB_2 samples, pure and synthesized with different amount of carbon nanotubes, under the A-K approximation. The absence of week links and the relatively low anisotropy allow us to consider the system under study as a bulk 3D superconductor with orientation-averaged J_c and U_c. A creep analysis was performed considering these "mean" isotropic variables. In Sec. II experimental details are described. In Sec. III the results are presented and discussed in Sec. IV. In Sec. V we present an analysis that allows us to identify the region where the A-K model is valid. Conclusions are summarized in Sec. VI.

II. EXPERIMENTAL

MgB_2 samples used were prepared by solid-state reaction with magnesium (−325 mesh, 99%), amorphous boron (99%), and double-walled carbon nanotubes (DWCNT; diameter 1.3–5 nm, length 50 μm, 90%, Aldrich) as starting materials.[8] The powders were ground inside a glove box and pressed under ~500 MPa into small pellets with dimensions of 6 mm in diameter and ~4 mm in thickness, wrapped together with extra 20 at % *Mg* turnings (99.98% Puratronic) in *Ta* foil and then placed in an alumina crucible inside a tube furnace in flowing Ar/H_2 at 900 °C for 30 min.

Samples with 0%, 1%, 2.5%, 5%, 7.5%, and 10% of CNT addition have been characterized. AC susceptibility sample characterization was carried out in a 9 T Quantum Design Physical Properties Measurement System (PPMS). The first harmonics of the AC susceptibility were normalized in such a way that the in-phase components χ' vary between –1 (ac field fully screened) and 0 (ac full penetration).

The magnetization measurements were carried out in a Quantum Design Magnetic Properties Measurement System (MPMS) model MPMS XL 7*T* SQUID based magnetometer. A scan length of 3 cm was used in order to minimize the effects due to the nonuniformity of the applied magnetic field (H), which was applied parallel to the longest axis of the sample. Isothermal magnetization loops $M(H)$ were measured to calculate J_c using the critical state model. Time-dependent data were taken with a protocol similar to that described in Ref. 18. For each relaxation measurement, the samples were first cooled and stabilized at the measurement temperature. Then the field was first raised up to a high field (5–6 T) and then lowered to the measuring field to assure that the sample was fully penetrated. Additional measurements were performed in the upper and lower magnetization branches to subtract the reversible magnetization and any background signal. We checked for and ruled out any effects due to the superconducting magnet relaxations (H variations during the measurement time) that could lead to spurious changes in the magnetization of the samples.

III. RESULTS

Samples have been characterized by AC susceptibility and magnetization measurements. In Figure 1, as an example, the first harmonic of the ac susceptibility is plotted as a function of temperature for a pure sample and for a sample with 10% addition of CNTs. These measurements were performed with a fixed AC amplitude h_a at various DC fields H (Fig. 1(a)) and at different AC fields (Fig. 1(b)). Even if there is a clear decrease in T_c with doping, the transitions at $H = 0$ are sharp in all the samples, indicating homogeneous superconducting properties in the macroscopic scale. No structure in the transition is observed when increasing both the AC and the DC field, indicating that the grain boundaries do not significantly destroy the superconducting properties in these ceramic samples. This fact allows us, in principle, to apply the theory, and data analysis developed to study vortex dynamics in homogeneous superconductors such as single crystals having in mind that, in the present case, grain with different orientations will surely have different properties and that our results are valid for mean properties in the macroscopic scale.

The critical current density $J_c(t)$ has been calculated from the measured magnetic moment using the relationship for a sample with rectangular cross section in the critical state following the Bean model.[19] At low fields the large magnetization values result in a non negligible difference between the average internal field $\langle B \rangle(H)$ in the upper and lower branches of the magnetization loop $M(H)$. This fact

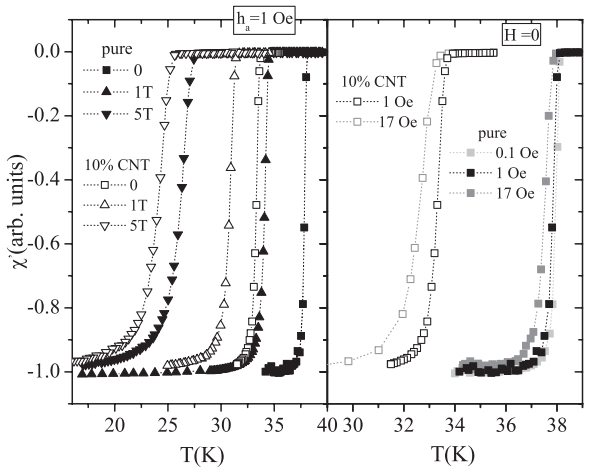

FIG. 1. In-phase component of the AC susceptibility χ' as a function of temperature for a pure sample and for a sample with 10% of CNT addition at fixed amplitude at various DC fields $\mu_0 H$ (a) and at $H = 0$ and various h_a (b). The transitions at $H = 0$ are sharp in all the samples, indicating homogeneous superconducting properties at the macroscopic scale.

and the strong dependence of $J_c(B)$ produce an asymmetric $M(H)$ loop with higher magnetization values in the lower branch. As has been suggested in the earlier work of Kim,[20] the average magnetic field in the upper and lower branches can be estimated by $\langle B\rangle \simeq \mu_0 H \pm M(H)/2$ and a quasi-symmetric loop $M(\langle B\rangle)$ can be obtained. For fields $\mu_0 H \sim$ 1T and higher, where the creep studies are performed, the difference between $\langle B\rangle$ and $\mu_0 H$ in all the samples becomes negligible; therefore, the relaxation study and sample comparison can be done at fixed H.

As discussed in previous works,[7–9,24] CNT additions are capable of H_{c2} and J_c simultaneous improvement. On one hand, they partially dilute into the MgB_2 matrix, acting as a source of C that increases H_{c2}. On the other hand, the remaining CNT's increase the amount of pinning centers, being the optimum CNT amount temperature and field dependent. In the range of CNT additions between 1% and 10%, the "measured" critical current density at temperatures far below T_c is highest and quite similar for different amounts of CNTs. For $x > 0.10\%$, J_c decreases due to both a larger decrease in T_c and a probable deterioration of interconnectivity between grains denoted by higher resistivity values. Analogous results had been reported by Dou *et al.*[21] This fact is illustrated in Figure 2(a), where the experimental J_c obtained in samples with different densities of CNT, is plotted as a function of $\mu_0 H$ at $T = 5$ K and 20 K. It can be observed that the response for samples with 1% (light gray triangles) and 10% (gray squares) addition of CNT is very similar and robust. On the other hand, pure MgB_2 samples are not so robust, and after large periods of time (several month or years) the critical current density can slightly decrease. At low temperature (5 K), CNT addition enhances J_c for all the measured range of H while at higher temperature (20 K) the response of pure and CNT samples is quite similar at low H (up to $\mu_0 H = 2$ T).

The magnetic relaxation has been measured in pure MgB_2 and samples with CNT contents between 1% and 10% in the range between 5 K and 25 K at $\mu_0 H = 1$ T. The corresponding relaxation rate S has been obtained as the slope of lnJ vs lnt. An example of the fitting procedure is shown in the inset of Figure 3(a). Results are shown in the main panel of Figure 3(a) (full symbols). Samples with 2.5% and 5% of carbon nanotubes additions have also been measured and display similar results, not shown in the figure for clarity.

The first, expected result is that, as was described in the introduction, the S values are intermediate between those measured in low and high T_c materials. Regarding the effect of CNT addition, the $S(T)$ curves display approximately the same behavior for all the samples with CNTs. However, as an unexpected result, it can be observed that at $\mu_0 H = 1$T pure samples (circles and triangles in Figure 3(a)) that have a lower J_c (associated with a lower pinning) have also a lower relaxation (associated with a higher pinning energy U_c).

The behavior of the relaxation S as a function of the applied magnetic field at fixed temperature $T = 10$ K is shown in Figure 2(b). The relaxation increases with CNTs addition at low fields but decreases notably at the higher

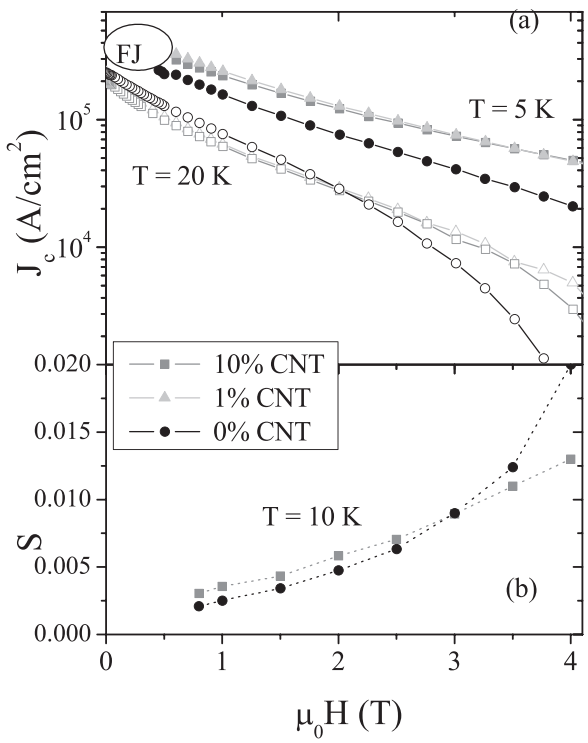

FIG. 2. (a) Experimental J_c obtained from $M(H)$ loops in samples with different amount of CNTs as a function of the applied field $\mu_0 H$ at $T = 5$ K and 20 K (b). Relaxation rate S as a function of $\mu_0 H$ for a pure (black dots) and a 10% CNT (gray squares) sample. $S(H)$ curves intersect around $\mu_0 H \sim 3$ T.

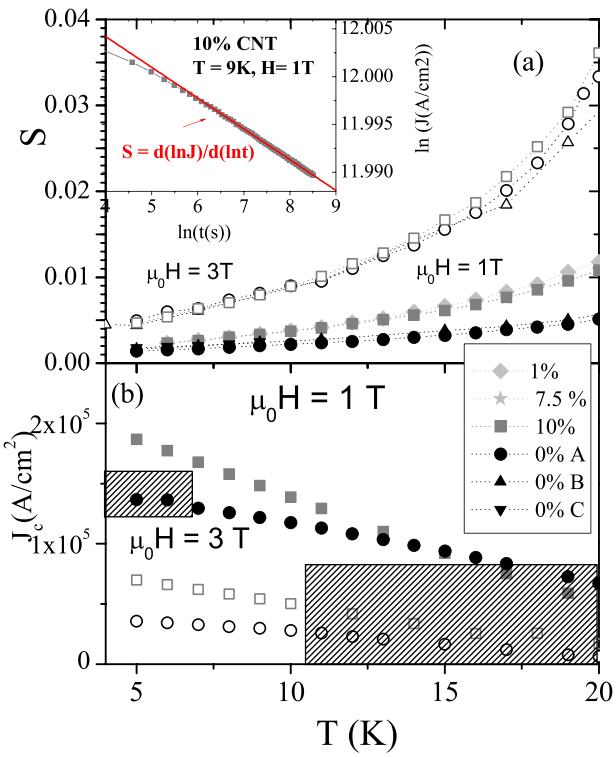

FIG. 3. (a) Relaxation rate S as a function of temperature for three pure MgB_2 samples (circles and triangles) and for samples with different doses of CNT: 1% (diamonds), 7.5% (triangles), and 10% (squares) at $\mu_0 H = 1$ T (full symbols) and $\mu_0 H = 3$ T (open symbols). Inset: an example of the procedure to estimate S is shown. (b) J_c as a function of T at the same fields for a pure sample A (circles) and a 10% CNT (squares) sample.

fields; around $\mu_0 H \sim 3$T all the samples with 0% and 10% CNT have approximately the same relaxation rate. In fact, relaxation rates for samples with and without CNTs at $\mu_0 H = 3$T are similar at all the temperatures bellow $T = 15$ K. This striking feature can be observed by comparing the $S(T)$ curves at $\mu_0 H = 3$T for 0% and 10% CNTs samples, plotted with open symbols in Figure 3(a).

In Figure 3(b) J_c for pure and 10% CNT sample is also plotted as a function of temperature at $\mu_0 H = 1$ T and 3 T. CNT addition enhances J_c at both fields bellow $T = 15$ K.

IV. DISCUSSION

The increase of S upon introduction of additional defects to increase pinning is not typically observed in other superconductors. For instance, irradiation of iron-based superconductors such as $Ba(FeCo)_2As_2$ produces increases in J_c but the relaxation rates either decrease[25] or remain constant.[26] On the other hand, $YBa_2Cu_2O_7(YBCO)$ samples with vastly different J_c values show very similar relaxation $S(T)$. One exception is the case of *YBCO* crystals with columnar defects where, together with the increase in J_c, a "peak" in $S(T)$ occurs.[15,18] However, that increase is observed over limited T and H ranges. The increase in $S(T,H)$ that we observe in our MgB_2 samples is a more general effect, taking place over a much broader T–H range. To get an understanding of the causes of the puzzle presented in the above section, the relaxation data in a pure and a 10% CNT samples were analyzed and compared.

The first consideration is that with the moderate relaxation rates measured, the strong temperature dependence $J_c(T)$ observed in Figure 3(b) cannot be explained assuming a T independent J_{c0} at low temperature. Thus, an intrinsic $J_{c0}(T)$ dependence must be taken into account, and the measured J_c would be similar to the true critical current density $J_{c0}(T)$. Therefore, experimental data were analyzed at each temperature assuming the validity of the A-K approximation $J_c \sim J_{c0}$. A novel procedure that is presented in Sec. V has been developed to check the consistence of this assumption.

In the general case,[13] the relaxation rate $S = -d(\ln(J))/d(\ln(t))$ is related to the pinning energy by

$$\frac{1}{S} = \frac{U_c(T;B)}{kT} + \mu \ln(1 + t/t_0) \sim \frac{U_c(T;B)}{kT} + \mu \ln(t/t_0), \quad (3)$$

where $t \gg t_0$ and $\ln t_0 \sim \ln(\tau_0 kT/J_{c0}|\partial J_c/\partial t|)$ is approximated as a constant. This expression should be valid in all the current density range, including the A-K regime.[17]

At low temperature $U_c/kT \gg 1$ and, as a good approximation,

$$\frac{1}{S} \sim \frac{U_c(T;B)}{kT}. \quad (4)$$

In Figure 4 the resulting pinning energies obtained from Eq. (4) are plotted as a function of temperature for pure and 10% CNT samples, at $\mu_0 H = 1$ T and 3 T. In the dashed regions marked in Figures 3(b) and 4, the results are not consistent with the A-K approximation. In favor of a continuity

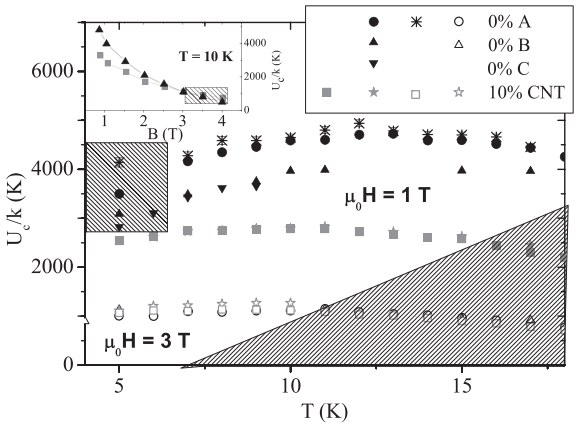

FIG. 4. Estimated pinning energies $U_c/k = T/S$ as a function of temperature for three pure (circles and triangles) and a 10% CNT sample (squares) at $\mu_0 H = 1$ T (full symbols) and $\mu_0 H = 3$ T (open symbols). Asterisk and stars compare pinning energies estimated using Eq. (8). In the dashed region the A-K approximation is not consistent. Inset: Dependence of pinning energy with magnetic induction B.

in the argument, let for the time being accept this claim as a fact; it will be justified in Sec. V.

Figure 4 shows that, in the regions where the A-K approximation is valid, pinning energies remain nearly constant. Consistent with the relaxation rates, at $\mu_0 H = 1$ T, there is a clear decrease of U_c after CNT addition, whereas at $\mu_0 H = 3$ T the pinning energies match up. The field dependence of the pinning energies is displayed in the inset, showing that the difference between 0% and 10% CNT samples decreases with magnetic field up to $B \sim 3$ T.

In the following we present a discussion and a possible picture to explain our experimental results. The parameter U_c is associated with the pinning energy of a pinning volume that is determined by the competition between pinning and elastic energies. In a single vortex pinning regime the pinning length L_c is defined by the balance between the pinning and the line elastic energy of a vortex segment.[13] The Lorentz force over a vortex segment of length L_c is $F_L \sim (1/c)\phi_0 J\, L_c$. On the other hand, in a pinning regime of vortex bundles, the pinning volume $V_c \sim L_c R_c^2$ involves the competition between pinning forces and lattice elastic moduli; in that case R_c is the distance where the autocorrelation function of the lattice displacement exceeds the range of the pinning potential r_p (Ref. 22) and the Lorentz force over a volume V_c is $F_L \sim (1/c)BJ\, V_c$. The B independence of pinning energies and critical currents has been often considered as the fingerprint of single vortex pinning. Obviously if pinning energies and critical currents were field independent we would be in the presence of a single vortex pinning regime. However, the inverse is not necessarily true: if pinning is strong enough the correlation volume could be small enough to involve only one vortex, but if the vortex distance is smaller than the penetration depth the effective pinning force acting over a vortex segment could be modified by the neighboring vortices. Therefore, a possible way to investigate this issue is by estimating the correlation volumes and lengths involved.

In a rough estimate, the pinning force is $F_p \sim U_c/r_p$. When J reaches the critical current density J_{c0}, the pinning

and Lorentz forces are balanced, and therefore the following relationships are obtained for the single vortex and bundle pinning regimes, respectively,

$$L_c(T,B) \sim \frac{cU_c(B,T)}{\xi(T)\phi_0 J_{c0}(B,T)}, \tag{5}$$

$$V_c(T,B) \sim \frac{cU_c(B,T)}{Br_p J_{c0}(B,T)}, \tag{6}$$

where r_p is generally a fraction of the lattice constant ($r_p \sim a_0/4$) and in the limit of a dilute vortex lattice reaches the coherence length $\xi(T)$.

In previous work,[7] we have presented H_{c2} measurements in MgB_2 with different amounts of CNTs, and we have found that $H_{c2}(T)$ fits very well the function proposed in Ref. 23. We have now estimated $\xi(T)$ from $H_{c2}(T)$ for the as grown samples and for samples with 10%*CNT*. Again, both H_{c2} and ξ are related with mean values, averaged over the various grain orientations. Using this $\xi(T)$ dependence (inset in Figure 5), and considering $J_{c0} = J_c$ we have estimated $L_c(T,B)$ from our data using Eq. (5). Results are shown in the main panel of Figure 5, where L_c is plotted as a function of temperature at $\mu_0 H = 1$ T and 3 T for both samples. Error bars take into account the possible difference between J_c and J_{c0} (we will admit a 10% difference to validate the A-K regime). Horizontal dashed lines indicate the spread of the reported grain size L_g. (150 nm $< L_g <$ 800 nm in virgin samples and 100 nm $< L_g <$ 500 nm in samples with CNTs).[24] It can be seen that if a single vortex pinning regime were present, the correlation length would be similar to grain size, slightly smaller in the samples with CNTs. L_c increases with temperature and magnetic field, until it exceeds the grain size, situation that striking matches with the limit of the validity of the A-K regime. Note that L_c is estimated solely from measurements of critical fields and vortex pinning and, in principle, could take any value between ξ to ∞ (in practice, the sample size). The coincidence of L_c with the grain sizes is remarkable, strongly suggesting that the pinning domains are constrained to single grains.

On the other hand, under the supposition of a pinning regime of vortex bundles and assuming $r_p \sim a_0/4$, V_c can be estimated from Eq. (6). Results are shown in Figure 6(a) and compared with the grain size and the volume of a cube of side a_0. In this picture V_c should be smaller in samples with CNTs and decreases at higher fields, contrary to the expectation in the theory of vortex bundles in the presence of random pinning centers.[13] That is not surprising because in our samples strong pinning centers are present, and grain boundaries probably influences the correlation volume. Grains are however larger than the estimated correlation volumes. Therefore, let us assume that the grain size limits only the longitudinal correlation length L_c. The correlation volume can be expressed in term of the transverse and longitudinal correlation lengths as $V_c \sim L_c R_c^2$. The area of a the correlation volume R_c^2 can be estimated by considering $L_c \sim L_g$. The estimated correlation areas are shown in Figure 6(b) for both samples as a function of temperature and compared with the area occupied by a single vortex at $\mu_0 H = 1$ T and 3 T. Error bars take into account the B distribution inside the sample ($\Delta B \sim \pi M$) and the spread in L_g. The resulting areas are in all the cases smaller than the region occupied by one vortex and, therefore, inconsistent with a vortex bundle pinning regime. Again, once the estimated area becomes larger than a_0^2 results are inconsistent with the A-K approximation (dashed region; see Sec. V).

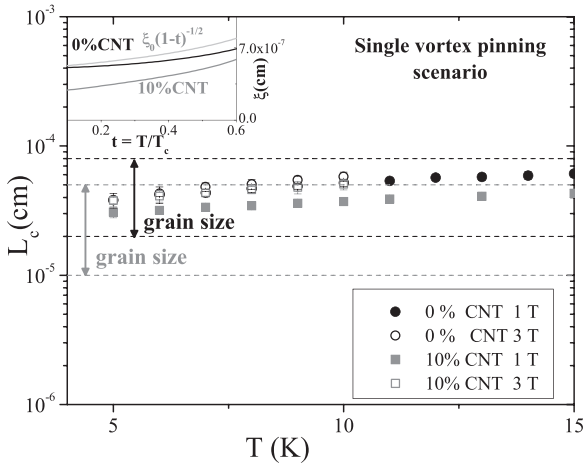

FIG. 5. Correlated pinning length L_c estimated assuming a single vortex pinning scenario in 10% CNT (gray squares) and as-grown samples (black circles) using Eq. (5). Dashed lines indicate the upper and lower limit of reported grain size L_g. Inset: coherence length ξ as a function of T calculated from H_{c_2} (Refs. 7 and 23).

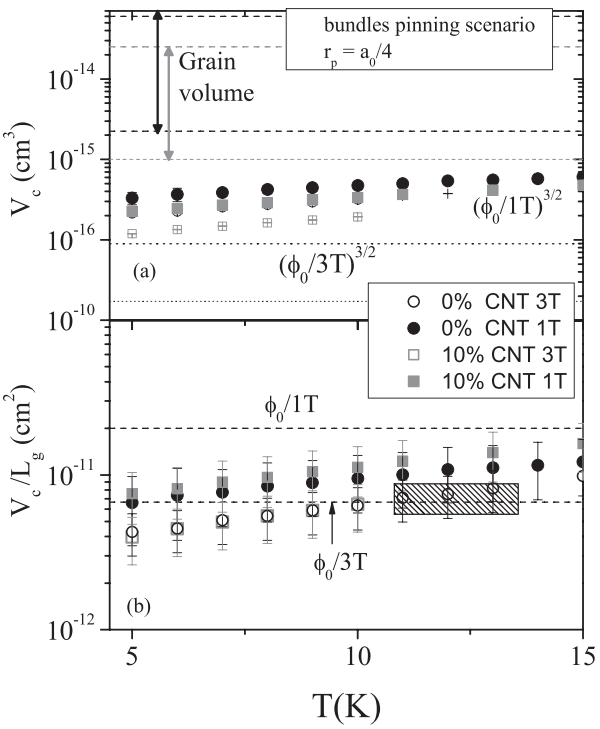

FIG. 6. (a) Correlated pinning volume V_c estimated assuming a vortex bundle pinning scenario in 10% CNT (gray squares) and as-grown samples (black circles) using Eq. (6) compared with the grain volume (gray and black dashed lines) and the volume of a cube with side a_0 at $B = 1$ T and 3 T. (b) Estimated correlated pinning area R_c^2 assuming $L_c = L_g$ compared with the area occupied by a single vortex at $B = 1$ T and 3 T.

From the above results, a pinning regime of small isotropic bundles containing a few vortices, in which the correlation volume anomalously decreases with B (Figure 6(a)), cannot be discarded. However, the most consistent picture indicates that in the region of small creep, where the A-K approximation is valid, a single vortex pinning regime with correlation length limited by the grain size (Figure 5) holds. As vortices are close enough, vortex-vortex interactions are not negligible, and the effective pinning energy U_c diminishes with B. This effect is stronger in pure samples. Because CNT addition reduces the mean grain size, the pinning correlation length is reduced in these samples. However, CNT addition not only decreases the grain size and correlation length but also reduces the coherence length ξ. This fact is probably the main responsible for the increase in the critical current density.

V. A-K MODEL CONSISTENCE

In this section we present a method to check the consistence of the A-K approximation. The procedure is applied to our results and allows us to discard, within an experimental criterion, data where the A-K model is not consistent (dashed regions in Figures 3, 4, and 6).

In the A-K condition $J_{c0} - J_c \ll J_{c0}$, the function $U(J)$ can be linearized to the first order in $(J_{c0} - J_c)$ to give the expression (2). The integration of Eq. (1) using Eq. (2) gives the well known logarithmic decay of the experimental critical current density with time. A mayor difficulty to directly decide the validity of the A-K approximation from the relaxation data at a single temperature is the extremely large time needed to reliably determine this logarithmic decay.

An alternative method, similar to that developed by Maley[27] for the case of giant creep, consists of taking the logarithmic expression of Eq. (1)

$$\frac{U(J_c,T,B)}{kT} = -\ln|\partial J_c/\partial t| + \ln C_j, \tag{7}$$

together with the A-K expression for the activation barrier (Eq. (2)), to obtain a linear dependence between J_c and $\partial J_c/\partial t$ that results in

$$J_c(t) = \frac{kT\,J_{c0}(T,B)}{U_c(B,T)}\ln|\partial J_c/\partial t| + J_{c0}(T,B)(1 - (\ln C_j)kT/U_c). \tag{8}$$

Due to the numerical differentiation, this method has a greater error in the calculation of the pinning energy but allows estimating $J_{c0}(T,B)$. The resulting fitting parameters must be consistent with the A-K conditions and with those obtained by using Eq. (4). If these two conditions are not fulfilled some of the assumptions will be wrong, and the A-K analysis should not be valid.

At each temperature $J_c(t)$ has been plotted as a function $ln(-\partial J/\partial t)$ (an example is shown the inset of Figure 7). By estimating $\ln C_j$, the true $J_{c0}(T)$ can be extracted from the intercept using Eq. (8). The easier assumption, using the fact that $\ln C_j \ll kT/U_c$, is to neglect $\ln C_j$. This procedure allows a reasonable estimation of $J_{c0}(T)$ but will underestimate the small difference $(J_{c0} - J_c)(T)$. It is possible to roughly estimate C_j from the expression in Ref. 13 (p. 1350), $C_j \sim J_c/\tau_0$ with $\tau_0 \sim \pi d^2/2c^2H^2\rho_{FF}$, being d the characteristic sample dimension, c the speed of light, ρ_{FF} the flux flow resistivity, and H expressed in Oe. This gives $\tau_0 \sim 10^{-4}s$ for our experimental situation, although this value could drop to $10^{-6}s$, depending on the reported resistivity.

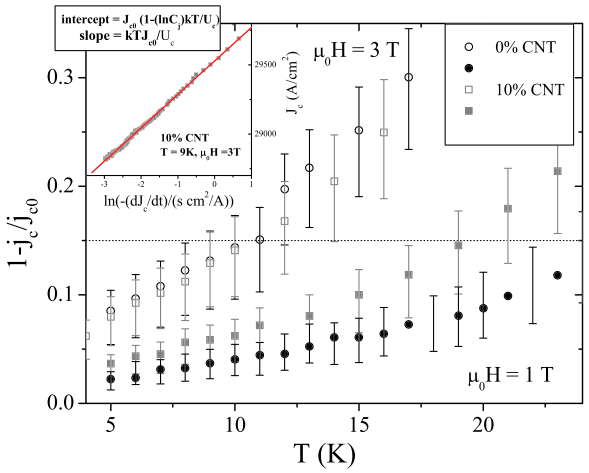

FIG. 7. Ratio $(J_{c0} - J_c)/J_{c0}$, where J_c and J_{c0} are the measured and the estimated "true" critical current densities, in the same samples used to build the previous figures The dashed line indicates the criterion to validate the A-K approximation. Inset: Example of fitting procedure using Eq. (8) to estimate U_c/k (asterisk and stars in Figure 4) and J_{c0} (main panel).

In Figure 7 the estimated true critical current density J_{c0} is compared with the measured critical current density J_c (the first point measured in the $J_c(t)$ relaxation) by plotting $(J_{c0} - J_c)/J_{c0}$ as a function of temperature for a pure sample (sample A in Figure 3) and a 10% CNT sample, at $\mu_0 H =$ 1 T and 3 T. Error bars take into account the uncertainty in C_j (from $\ln C_j = 0$ to $\ln(C_j \sim J_c[\mathrm{A/cm^2}]10^6)$ discussed in the above paragraph. Taking a 15% criterion to determine the limit of the A-K condition $(J_{c0} - J_c) \ll J_{c0}$, the resulting $J_{c0}(t)$ is consistent below the temperature where each experimental curve crosses the doted horizontal line.

From the slope $A = kTJ_{c0}/U_c$ in Eq. (8) the pinning energy $U_c/k = AJ_{c0}T$ can be extracted and compared with T/S for these samples. Results are shown with asterisk and stars in Figure 4. As can be observed (with exception of the lower temperatures data in the pure sample at $\mu_0 H = 1$ T) pinning energies obtained from both methods are very similar, and this validates the fitting procedures, including the estimation of $J_{c0}(T)$ from Eq. (8).

The unexpected drop in U_c at the lower temperatures data in the pure sample at $\mu_0 H = 1$ T, together with the inconsistence of the analyzed data, could imply the presence of another relaxation mechanism, perhaps associated with macroscopic flux jumps.

VI. CONCLUSIONS

Magnetic relaxation in bulk MgB_2 samples with and without CNT additions has been measured at various temperatures and magnetic fields, and the corresponding mean

critical current density has been calculated. The current decay in time is quite similar in all the samples with CNT amounts between 1% and 10%.

A detailed creep analysis has been carried out in a pure sample and in one with 10% of carbon nanotubes. The analysis has been performed under the Anderson-Kim approximation, valid in the limit where the measured critical current density J_c is similar to the "true" one J_{c0} that would be present in the absence of creep phenomena. In these samples, even at the lower temperatures, it is necessary to include an explicit field and temperature dependence for true critical current densities $J_{c0}(T,B)$.

Mean pinning energies have been calculated. By estimating approximately the volumes and/or correlated pinning lengths we conclude that the most consistent picture at low temperatures is a single vortex pinning regime, where the correlation length is limited by the grain size. Despite that, pinning energies decreases with magnetic field. This fact is not surprising because vortex densities are high enough to produce an effective pinning potential influenced by vortex interaction.

At low magnetic fields, CNT addition produces a decrease in the pinning energies (which increases the relaxation rates). However, the critical current density increases.

We conclude that the puzzle solution to explain the changes in the pinning properties with CNT addition is the combination of the reduction of the grain size (that decreases pinning energies) and coherence length (that increases the critical current density).

The region of validity of the A-K approximation has been tested by obtaining the pinning parameters with an alternative method. The consistence of the fitting parameters with the A-K limit has been required. The coincidence between the region where the A-K approximation is valid and that one where the correlation length is smaller than the grain size (see Figure 6) suggest that probably the grain boundaries modify the creep mechanism and pinning regime. A method to analyze the relaxation data in the high temperature region of compounds with intermediate creep, beyond the A-K approximation, as well as a model to describe pinning and relaxation in the presence of grain boundaries would be suitable to understand relaxation processes in the whole phase diagram of these materials.

ACKNOWLEDGMENTS

This work was partially supported by CONICET, ANPCyT, UNCuyo, and UBACyT, Argentina, and the U.S. DOE, Office of Basic Energy Sciences, Division of Materials Sciences and Engineering, USA.

[1]J. Nagamatsu, N. Nakagawa, T. Muranaka, Y. Zenitani, and J. Akimitsu, Nature (London) **410**, 63 (2001).
[2]C. Buzea and T. Yamashita, Supercond. Sci. Technol. **14**, R115 (2001).
[3]D. C. Larbalestier *et al.*, Nature (London) **410**, 186 (2001).
[4]H. Kumakura, H. Kitaguchi, A. Matsumoto, and H. Hatakeyama, Appl. Phys. Lett. **84**, 3669 (2004); S. X. Dou, S. Soltanian, J. Horvat, X. L. Wang, P. Munroe, S. H. Zhou, M. Ionescu, H. K. Liu, and M. Tomsic, *ibid.* **81**, 3419 (2002); S. X. Dou, V. Braccini, S. Soltanian, R. Klie, Y. Zhu, S. Li, X. L. Wang, and D. Larbalestier, J. Appl. Phys. **96**, 7549 (2004).
[5]W. K. Yeoh, J. H. Kim, J. Horvat, S. X. Dou, and P. Munroe, Supercond. Sci. Technol. **19**, L5–L8 (2006); A. Vajpayee, V. P. S. Awana, S. Yuc, G. L. Bhalla, and H. Kishan, Physica C **470**, S653 (2010).
[6]A. Serquis, X. Z. Liao, Y. T. Zhu, J. Y. Coulter, J. Y. Huang, J. O. Willis, D. E. Peterson, F. M. Mueller, N. O. Moreno, J. D. Thompson, V. F. Nesterenko, and S. S. Indrakanti, J. Appl. Phys. **92**, 351 (2002).
[7]A. Serquis, G. Serrano, M. S. Moreno, L. Civale, B. Maiorov, F. Balakirev, and M. Jaime, Supercond. Sci. Technol. **20**, L12 (2007).
[8]G. Serrano, A. Serquis, S. X. Dou, S. Soltanian, L. Civale, B. Maiorov, F. Balakirev, and M. Jaime, J. Appl. Phys. **103**, 023907 (2008).
[9]G. Serrano, A. Serquis, L. Civale, B. Maiorov, T. Holesinger, F. Balakirev, and M. Jaime, Int. J. Mod. Phys. B **23**, 3465 (2009).
[10]A. A. Golubov, J. Kortus, O. V. Dolgov, O. Jepsen, Y. Kong, O. K. Andersen, B. J. Gibson, K. Ahn, and R. K. Kremer, J. Phys.: Condens. Matter **14**, 1353 (2002); A. Gurevich, S. Patnaik, V. Braccini, K. H. Kim, C. Mielke, X. Song, L. D. Cooley, S. D. Bu, D. M. Kim, J. H. Choi, L. J. Belenky, J. Giencke, M. K. Lee, W. Tian, X. Q. Pan, A. Siri, E. E. Hellstrom, C. B. Eom, and D. C. Larbalestier, Supercond. Sci. Technol. **17**, 278 (2004).
[11]I. A. Ansari, M. Shahabuddin, N. S. Alzayed, A. Vajpayee, V. P. S. Awana, and H. Kishan, Physica C **470**, 369 (2010); K. E. Taylan, A. Surdu, A. Sidorenko, and E. Yanmaz, J. Supercond. Novel Magn. **25**, 1761 (2012).
[12]B. Maiorov, S. A. Baily, H. Zhou, O. Ugurlu, J. A. Kennison, P. C. Dowden, T. G. Holesinger, S. R. Foltyn, and L. Civale, Nat. Mater. **8**, 398 (2009); N. Haberkorn, M. Miura, B. Maiorov, G. F. Chen, W. Yu, and L. Civale, Phys. Rev. B **84**, 094522 (2011).
[13]G. Blatter, M. V. Feigel'man, V. B. Geshkenbein, A. I. Larkin, and V. M. Vinokur, Rev. Mod. Phys. **66**, 1125 (1994).
[14]Y. Yeshurun, A. P. Malozemoff, and A. Shaulov, Rev. Mod. Phys. **68**, 911 (1996).
[15]J. R. Thompson, Y. Sun, D. Christen, L. Civale, A. Marwick, and F. Holtzberg, Phys. Rev. B **49**, 13287 (1994); J. R. Thompson, E. L. Krusin, L. Civale, G. Blatter, and C. Field, Phys. Rev. Lett. **78**, 3181 (1997).
[16]R. Prozorov, N. Ni, M. A. Tanatar, V. G. Kogan, R. T. Gordon, C. Martin, E. C. Blomberg, P. Prommapan, J. Q. Yan, S. L. Bud'ko, and P. C. Canfield, Phys. Rev. B **78**, 224506 (2008).
[17]P. W. Anderson and Y. B. Kim, Rev. Mod. Phys. **36**, 39 (1964).
[18]See, for example, L. Civale, G. Pasquini, P. Levy, G. Nieva, D. Casa, and H. Lanza, Physica C **263**, 389 (1996).
[19]E. H. Brandt, Phys. Rev. B **52**, 15442 (1995).
[20]Y. B. Kim, C. F. Hempstead, and A. R. Strnad, Phys. Rev. **129**, 528 (1963).
[21]S. X. Dou, W. K. Yeoh, J. Horvat, and M. Ionescu, Appl. Phys. Lett. **83**, 4996 (2003); W. K. Yeoh, J. Horvat, S. X. Dou, and V. Keast, Supercond. Sci. Technol. **17**, S572 (2004).
[22]E. H. Brandt, J. Low Temp. Phys. **64**, 375 (1986).
[23]V. Braccini, A. Gurevich, J. E. Giencke, M. C. Jewell, C. B. Eom, D. C. Larbalestier, A. Pogrebnyakov, Y. Cui, B. T. Liu, Y. F. Hu, J. M. Redwing, Q. Li, X. X. Xi, R. K. Singh, R. Gandikota, J. Kim, B. Wilkens, N. Newman, J. Rowell, B. Moeckly, V. Ferrando, C. Tarantini, D. Marré, M. Putti, C. Ferdeghini, V. R. Erqi, and E. Haanappel, Phys. Rev. B **71**, 012504 (2005).
[24]A. Serquis and G. Serrano, *Doping Effects on the Superconducting Properties of Bulk and PIT MgB_2* (Superconductor Research Nova Science Publishers, 2008), Vol. 221.
[25]Y. Nakajima, Y. Tsuchiya, T. Taen, T. Tamegai, S. Okayasu, and M. Sasase, Phys. Rev. B **80**, 12510 (2009); Tamegai *et al.*, Supercond. Sci. Technol. **25**, 084008 (2012) and references therein.
[26]N. Haberkorn, B. Maiorov, I. O. Usov, M. Weigand, W. Hirata, S. Miyasaka, S. Tajima, N. Chikumoto, K. Tanabe, and L. Civale, Phys. Rev. B **85**, 014522 (2012).
[27]M. P. Maley, J. O. Willis, H. Lessure, and M. E. McHenry, Phys. Rev. B **42**, 2639 (1990).